Applied Surface Science 673 (2024) 160906

Contents lists available at ScienceDirect

Applied Surface Science

journal homepage: www.elsevier.com/locate/apsusc

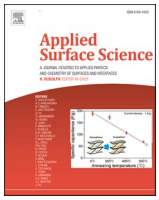

Full Length Article

Effect of gold nanoparticles on SiO_2@g-C_3N_4 catalyst for the degradation of amoxicillin

L. Santamaría [a,b,*], S.A. Korili [b], A. Gil [b], J.M. López-de-Luzuriaga [a], M. Monge [a,**]

[a] Departamento de Química, Centro de Investigación En Síntesis Química (CISQ), Complejo Científico Tecnológico, Universidad de La Rioja, Madre de Dios 53, 26006 Logroño, Spain
[b] INAMAT^2,-Departamento de Ciencias, Edificio de Los Acebos, Universidad Pública de Navarra, Campus de Arrosadía E-31006, Pamplona, Spain

ARTICLE INFO

Keywords:
SiO_2 nanotubes
gold NP-doped graphitic carbon nitride
Superoxide radicals ($\cdot O_2^-$)
Photocatalytic antibiotic degradation

ABSTRACT

Gold nanoparticles in different proportions (0.5 and 1 %) have been grafted at the surface of a SiO_2@g-C_3N_4 nanotube-based composite (SiO_2 nanotubes obtained from halloysite clay) and also g-C_3N_4 (for comparison purposes) to test their degradation capacity over the antibiotic amoxicillin proving that the introduction of these nanoparticles on the catalyst modifies the degradation mechanism followed by the pollutant. Results obtained show that the introduction of the appropriate percentage of gold NPs in the composite improves amoxicillin degradation efficiency and establish a direct correlation between the presence of gold NPs and the production of $\cdot O_2^-$.

1. Introduction

As the clean water shortage becomes more evident, wastewater treatments must reinforce efforts to release to the environment cleaner water. Nowadays, the ever-growing use of antibiotics is yet to be matched with a water treatment able to prevent them from being released to the ecosystems. The main legal instrument for water protection in Europe, the Water Framework Directive [1] aims at improving ecological and chemical status of surface water. In order to increase the available information on recognizing the substances of greatest concern, the surface water watch list was established in 2013, with updates every two years. Amoxicillin was included in the 2018 list [2] with concerns over the occurrence and spread of antimicrobials in the environment, in line with the European One Health Action Plan against Antimicrobial Resistance (AMR) [3]. This ability of the microorganisms to become resistant to the antimicrobial to which they were previously susceptible, has reached alarming levels worldwide [4] and it has been predicted that AMR may cause more deaths than cancer by 2050 [5] Amoxicillin, a β-lactam antibiotic, is hardly metabolized after its consumption and around 86 % is excreted [6] and, as well as most antibiotics, is recalcitrant when being subjected to conventional wastewater treatments [7].

Advanced oxidation processes have generated great expectations in the last decade. Although they can be energy-demanding systems, its main advantage is the destruction of the organic compound treated, which solves the problems presented with the use of other cleaning systems based on membranes or adsorption mechanisms. These do not eliminate the pollutant and need a secondary step for the system reutilization or further separation is needed to recover fresh water [8]. The use of carbon nitride as photocatalyst for wastewater treatment has generated great progress recently [9–13] as its capacity to absorb visible light, sets this semiconductor one step ahead of only-UV-light-absorbing TiO_2 [14]. However, the visible light absorption capacity of g-C_3N_4 is very limited: its swift electron-hole recombination capacity and wide band gap raise a challenge regarding and efficient solar-energy utilization. Both are tried to be tackled following different strategies: formation of heterojunctions, surface modification, metal doping or localized surface plasmon resonance (LSPR) enhancement [15]. Surface modification has proven to increase the BET surface of the semiconductor and, thus, the number of surface reactive sites. The use of a support (usually both affordable and green) in which g-C_3N_4 can deposit, ameliorates agglomeration issues, as it acts as a settle guide [16,17]. The support used in the starting composite of this work (SiO_2 nanotubes) has been

* Corresponding author at: INAMAT2,-Departamento de Ciencias, Edificio de los Acebos, Universidad Pública de Navarra, Campus de Arrosadía E-31006, Pamplona, Spain.
** Corresponding author at: Departamento de Química, Centro de Investigación en Síntesis Química (CISQ), Complejo Científico Tecnológico, Universidad de La Rioja, Madre de Dios 53, 26006 Logroño, Spain.
E-mail addresses: leticia.santamaria@unavarra.es (L. Santamaría), miguel.monge@unirioja.es (M. Monge).

https://doi.org/10.1016/j.apsusc.2024.160906
Received 29 May 2024; Received in revised form 26 July 2024; Accepted 3 August 2024
Available online 5 August 2024

proven to both increase the BET surface and reduce the electron-hole recombination of carbon nitride. Different SiO_2 structures such as spheres, hollow spheres or aerogel have been proven to improve both TiO_2 and g-C_3N_4 catalytic efficiency [18–23]. The enhanced activity of the composite is mainly associated to its large surface area, thin g-C_3N_4 stack layers, and high separation efficiency of electron– hole pairs. The greater dispersion of the carbon nitride together with the porous and unilayered structure of the SiO_2 nanotubes facilitates the separation of charge carriers which translates into a quenched signal [24]. This may cause an increase in photocatalytic activity as the existence of the photoinduced electron-hole pairs is lengthened [25].

Doping the catalyst with noble metals (such as Au, Ag or Pt) can also significantly enhance the catalyst performance [26]. These plasmonic nanoparticles are known to be an efficient method to reduce the band gap of g-C_3N_4 which broadens the light absorption capacity and further increase its photocatalytic activity on the visible-light range [27–29]. They have a twofold role: the formation of the Schottky barrier which forms a pathway from the conduction band of the semiconductor to the nanoparticles, which act as electron sinks, and the LSPR from the nanoparticle to the semiconductor which can also reduce the charge recombination. The use of limited amounts of Au NPs and their role in the catalysis process in combination with g-C_3N_4 [30], carbon self-doping g-C_3N_4 [31] and in a dual ZnO/C_3N_4 catalyst [32] has been lately explored for hydrogen production and also in a combination with other plasmonic nanoparticles, like platinum [33].

In this work, gold nanoparticles were formed at the surface of a catalyst composed of graphitic carbon nitride (g-C_3N_4) 2D-nanosheets wrapped around silica nanotubes obtained from the acid activation of the clay halloysite. For comparison purposes, g-C_3N_4/Au NPs with no nanotubes were also synthesized and characterized (N_2 adsorption–desorption, PXRD, TEM, DRS, XPS, PL). Two gold percentages were chosen, 0.5 and 1 wt% of added metal content. The composites were tested for the degradation of a persistent emerging pollutant in water, antibiotic amoxicillin, under visible light. The degradation mechanism of the best performing sample (SiO_2@g-C_3N_4/Au 0.5 %) was studied with trapping experiments by the use of scavengers that were introduced to quench the photodegradation: triethanolamine for photoexcited holes (h^+), *tert*-butanol for hydroxyl radicals (·OH) and a N_2 atmosphere for superoxide radicals ($\cdot O_2^-$).

2. Experimental procedure

2.1. Materials

For the synthesis of Au nanoparticles, the precursor [Au(C_6F_5)(tht)] (tht = tetrahydrothiophene) was synthesized by standard procedures reported previously [34]. Triisopropylsilane (98 %) and tetrahydrofuran were provided by Sigma Aldrich and VWR Chemicals, respectively. Amoxicillin trihydrate was provided by FluoroChem. HPLC-grade acetonitrile was provided by Scharlab (Barcelona, Spain) and formic acid (98 %) for HPLC was from Fluka Analytical. Chemicals were used as received and no further purification was needed.

2.2. Nanocomposites synthesis

The composite synthesis process before the decoration with Au nanoparticles is described elsewhere [24]. In summary, halloysite clay (an aluminosilicate found naturally in a nanotube shape) was acid treated in order to strip the Al_2O_3 layer and obtain SiO_2 nanotubes which were then used as a support in which g-C_3N_4 could wrap around. The composition of the SiO_2@g-C_3N_4 sample is almost half in g-C_3N_4 (46 %). Two different percentages of gold were tested (0.5 and 1 wt%) using [Au(C_6F_5)(tht)] as organometallic precursor. This gold precursor is reduced in the presence of the SiO_2@g-C_3N_4 system. First, a suspension of either SiO_2@g-C_3N_4 or g-C_3N_4 was sonicated for 10 min with 10 mL of tetrahydrofuran in a round-bottomed flask. Then, 6,1/11.6 mg of [Au(C_6F_5)(tht)] with 80 mg of triisopropylsilane and 10 mL of tetrahydrofuran were added together to the flask. The suspension was stirred and heated under reflux at 70 °C for 1 h in dark conditions. The nanocatalyst was then filtered, obtaining a violet colored powder (see Image 1 and Fig. 1).

2.3. Characterization of the adsorbents

N_2 adsorption–desorption at -196 °C was used in order to assess the porosity and the crystallites surface of the samples. 0.4 g of each sample were placed in a Micromeritics ASAP 2020 Plus adsorption analyzer. Firstly, they were degassed at 200 °C for 24 h under vacuum as a pretreatment. The Brunauer-Emmett-Teller (BET) equation was used to determine the specific surface area using the adsorption data (range 0.05–0.20 of relative pressure). The *t-plot* method was used to estimate both the external surface area (*Sext*) and the micropore volumes (*Vμp*). Pore size distribution was derived from the adsorption branch of the isotherm by BJH (Barret–Joyner–Halenda) using Halsey–Faas correction. Powder X-ray diffraction (**PXRD**) diffractograms were obtained with a Bruker D8 Advance Eco X-ray diffractometer. In order to identify the crystalline phase of the samples, a Ni-filtered Cu Kα radiation (λ = 0.1548 nm) at a 2-theta range from 5 to 80° and a scanning rate of 2° (2θ)/min were used. The morphological characterization of the samples was carried out by Transmission Electron Microscopy (**TEM**). Samples dispersed in ethanol (2–3 drops) were drop-casted to carbon-coated Cu grids. The corresponding micrographs were acquired with a Tecnai T20 (ThermoFisher Scientific) at a working voltage of 200 kV. Diffuse reflectance UV–vis spectra (**DRS**) of the samples were recorded on a UV-3600 spectrophotometer (Shimadzu, Kioto, Japan) equipped with a Harrick Praying Mantis accessory. The Kubelka-Munk function was used to obtain the solid-state absorption spectra. X-ray photoelectron spectroscopy (**XPS**) analyses were carried out on a Versaprobe III Physical Electronics (ULVAC) spectrometer equipped with a monochromatized Al Kα X-ray source (1486.7 eV) in order to obtain the surface elemental composition. A pass energy of 224 eV was set for the general spectra and of 27 eV for the elementary spectra. The surface adventitious carbon peak, C 1 s at 284.5 eV, was used as a reference for all the binding energies. When required, spectra were deconvoluted with the CasaXPS 2.3.26 program (Casa Software Ltd., UK). A Shimadzu RF-6000 Spectrofluorophotometer was employed to record the excitation and emission spectra of the samples.

2.4. Amoxicillin photodegradation experiments

The photoreaction tests were performed using a Photolab Equipment

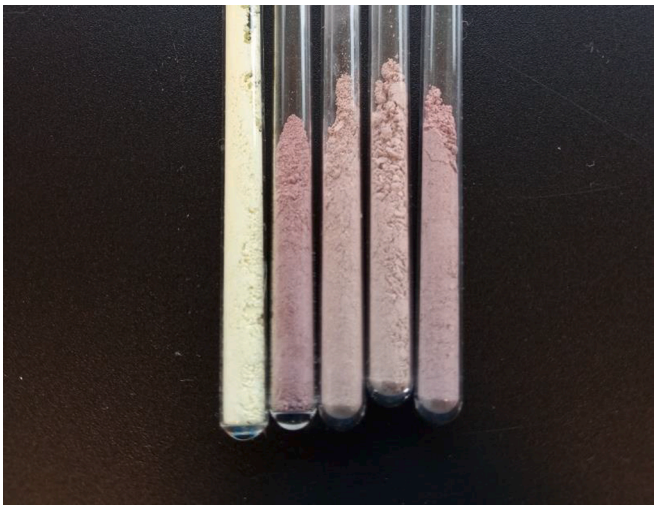

Image 1. G-c_3N_4, SiO_2@g-C_3N_4/Au 1 %, SiO_2@g-C_3N_4/Au 0.5 %, g-C_3N_4/Au 0.5 %, g-C_3N_4/Au 1 % samples.

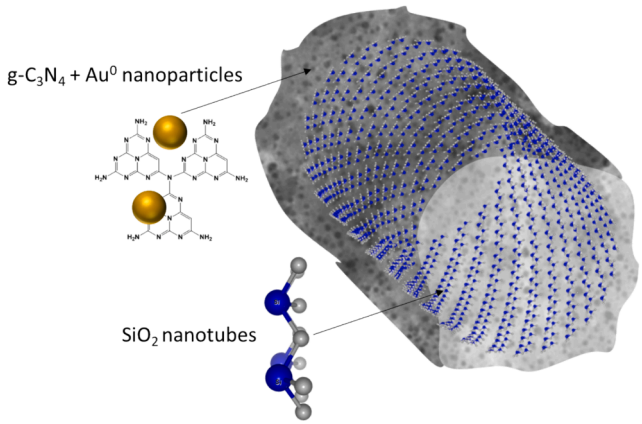

Fig. 1. Structure of the composite used as a catalyst.

(LED365-1/450–1/850-1cb, Apria Systems, Spain) equipped with three lamps providing visible, UV and IR light, respectively. IR light was kept unlit in order to perform there the adsorption experiments, in the absence of light. 20 mg of the catalyst was placed in a petri dish containing 20 mL of amoxicillin aqueous solution (5 ppm in Milli-Q water, neutral pH). The visible lamp (radiation of 124 W/m^2) was switched on and the photocatalyst performance was tested for 120 min under agitation. The monitoring of the antibiotic concentration was performed by withdrawing aliquots of 1 mL of the solution every 15 min. The aqueous solutions were then filtered (0.22 µmol, Durapore) and the drug concentration was determined with an Agilent modular 1100/1200 liquid chromatography system (Agilent Technologies, USA) equipped with a G1329A autosampler and a G1315 diode array detector and a Phenomenex Luna LC C18 100 \AA column. The mobile phase started 85 % of 0.1 % formic acid aqueous solution and 15 % acetonitrile. The total running time was 20 min with a 1.0 mL/min flow rate and an injection volume of 20 µL. Amoxicillin signal was measured at 228 nm. The catalytic photoreactions were carried out at natural pH and photolysis tests, in the absence of a catalyst, were also performed. The study of the active species responsible for the degradation procedure was performed with the help of trapping experiments. In order to quench hydroxyl radicals (·OH) and photogenerated holes (h^+), triethanolamine and *tert*-butanol, respectively, were added to the reactions to act as scavengers. N_2 atmosphere was also used to let out the oxygen present in the setup and test the presence of superoxide radicals (·O_2) [35–37].

3. Results and discussion

3.1. Catalysts characterization

The effect that the presence of nanoparticles had on the textural properties of the samples was examined with N_2 adsorption–desorption. The results obtained are displayed in Fig. 2 and Table 1. All the isotherms correspond to a type IV in the IUPAC classification [38], which are given by mesoporous adsorbents. The presence of a hysteresis loop in the 0.5–1.0 pressure range confirms the mesoporous structure of the samples (see Fig. 2a). The decoration of carbon nitride with gold nanoparticles can have different results in the BET surface of the samples, with studies reporting an important increase or decrease in their samples, while other reports no significant changes [39–41]. The BET surface of the g-C_3N_4 series seems to slightly increase with the presence of the NPs while in the SiO_2@g-C_3N_4 series has mixed effects. The Barrett-Joyner-Halenda (BJH) pore-size distributions of the samples (displayed in Fig. 2b) clearly reflects the difference between the series: while the g-C_3N_4 series has a linear distribution of mesopores, the SiO_2@g-C_3N_4 series shows that the amount of mesopores increases with the presence of the gold nanoparticles. A peak situated at the 11 nm pore diameter, corresponds to the mesoscopic lumen of the SiO_2 nanotubes

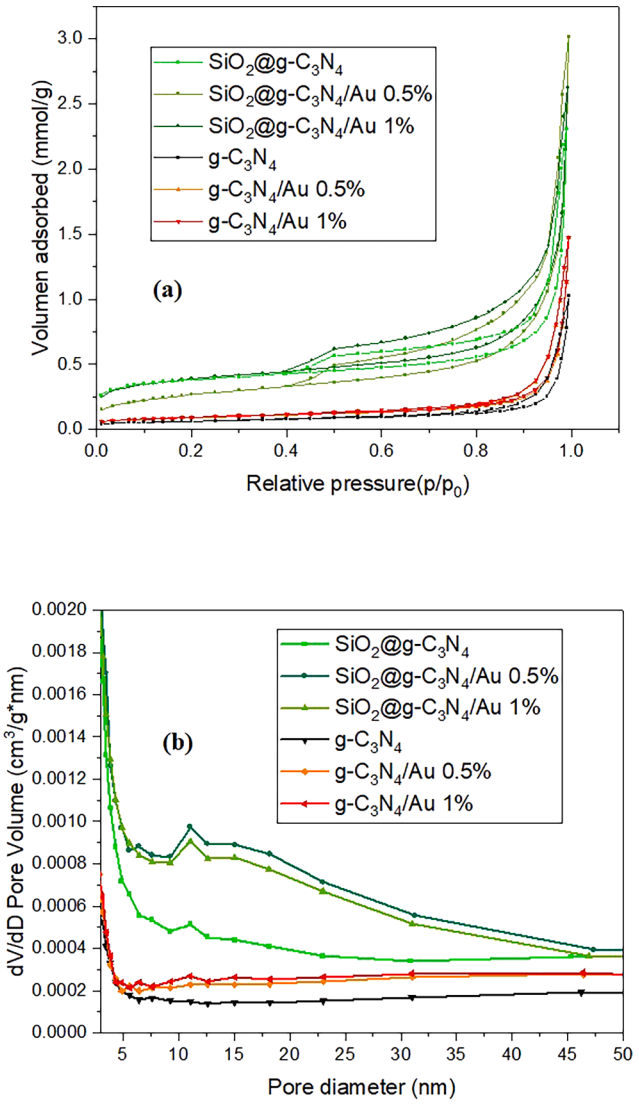

Fig. 2. The N_2 adsorption–desorption isotherms **(a)** and pore size distribution **(b)** of the samples.

Table 1
Textural properties of the halloysite/melamine-derived photocatalysts with different percentages of gold.

Sample	S_{BET} (m^2/g)	S_{ext} (m^2/g)
g-C_3N_4	5	4
g-C_3N_4 + Au 0.5 %	7	6
g-C_3N_4 + Au 1 %	7	6
SiO_2@g-C_3N_4	26	15
SiO_2@g-C_3N_4 + Au 0.5 %	21	21
SiO_2@g-C_3N_4 + Au 1 %	28	21

[42].

The PXRD diffractograms of the samples are displayed in Fig. 3. Samples with g-C_3N_4 and no nanotubes (g-C_3N_4/Au 0.5–1 %) show the typical diffraction peaks of carbon nitride: a peak situated at 12.9/12.8° was accorded to the interplanar packing of the tri-s-triazine unit of (1 0 0) plane and the broad peak at 26.3/27° was indexed to the staking (0 0 2) peak of the conjugated aromatic system (JCPDS card 87-1526). In both samples the presence of metallic gold can be observed with the peak situated at 38/38.3°, corresponding to the (1 1 1) plane of Au NPs (JCPDS card No. 04-0784). The sample with 1 % gold displays a bigger

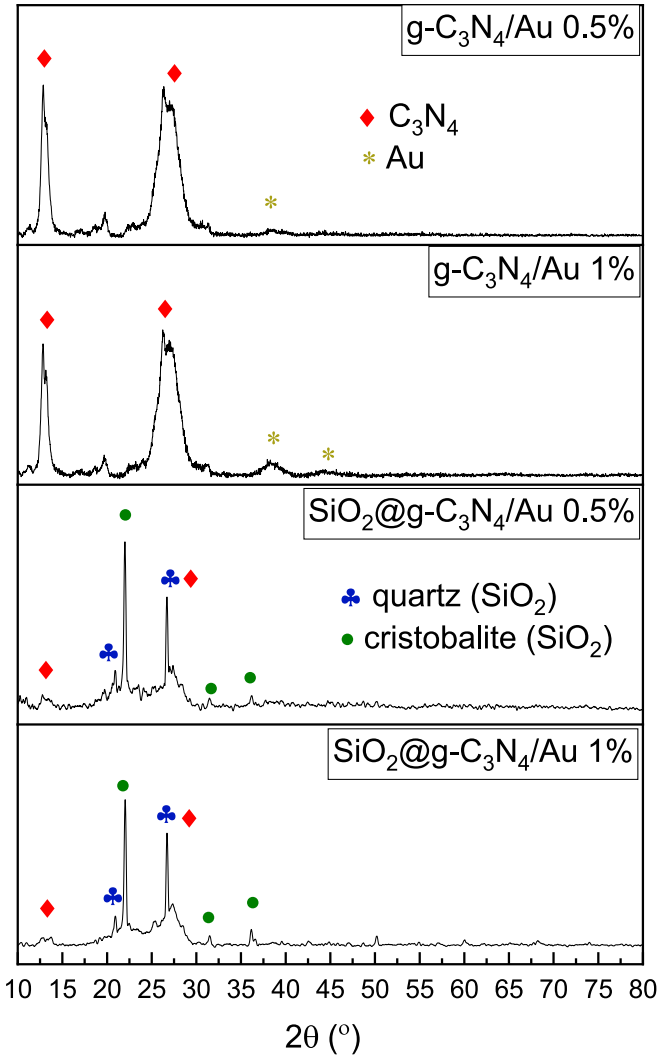

Fig. 3. Powder X-ray diffraction patterns of the C_3N_4/Au 0.5–1 % samples are displayed in the first two rows and those of SiO_2@g-C_3N_4/Au 0.5–1 % samples in the third and last row.

peak and also a peak situated at 45°, which matches to the (200) plane. The composites with nanotubes (SiO_2@g-C_3N_4/Au 0.5–1 %) feature in their most intense peaks the presence of silica arranged both as quartz with peaks at 20.9° and 26.7° corresponding to (100) and (101) planes, respectively (JCPDS card No. 046-1045) and cristobalite at 22° (101), 31.4 (102) and 36.1 (200) (JCPDS card No. 39-1425). The presence of both g-C_3N_4 is thus downsized and less evident, (002) peak appears together with quartz (101). Although the percentage of added gold is the same than in the g-C_3N_4/Au samples (see XPS results), its presence cannot be detected with PXRD in the samples with nanotubes.

Fig. 4 shows TEM images of the synthesized catalysts. The presence of nanoparticles is readily observable in all samples. The gold nanoparticles grafted on g-C_3N_4 display a very homogeneous shape and are well-distributed throughout the samples proving that the synthesis procedure was successful. The triazine groups of the g-C_3N_4 acted in all samples as a direct growth agent and thus, the size of the NPs was controlled without the need of a polymer, as proved previously in our group [43]. Although not shown in the PXRD analysis, the incorporation of the gold in the silica composite, does not seem to have any effect on either the distribution or the size of the nanoparticles. Both the size of the NPs (<10 nm) and their distribution are homogeneous. Sample g-C_3N_4/Au 1 % has an average size of 4.91 ± 1.7 nm while the samples with nanotubes have an average size of 3.56 ± 0.6 and 3.54 ± 1.2 nm for

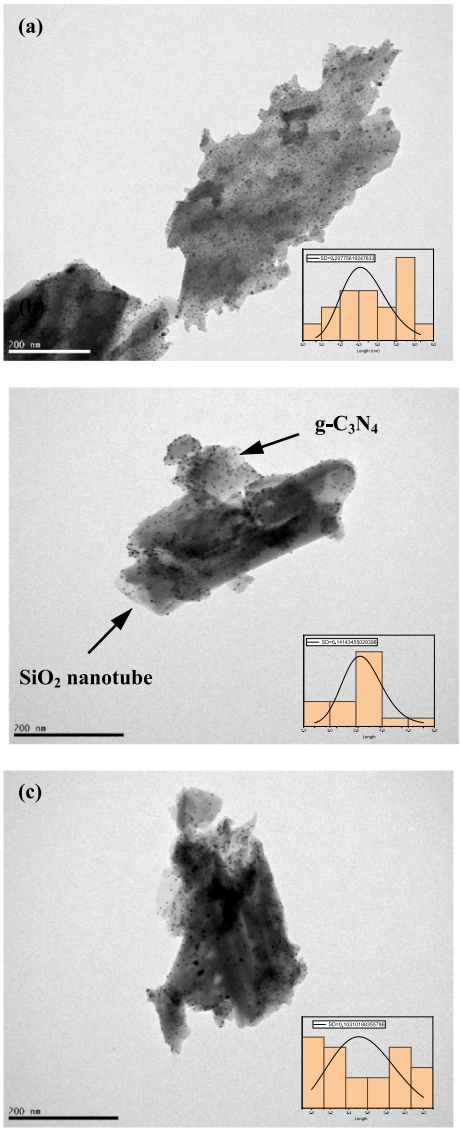

Fig. 4. TEM micrographs of the samples: g-C_3N_4/Au 1 % (a) SiO_2@g-C_3N_4/Au 0.5 % (b) SiO_2@g-C_3N_4/Au 1 % (c).

Au 0.5 % and 1 %, respectively. The presence of the nanotubes, which accounts for a smoother and more extended g-C_3N_4 distribution, could have contributed to a smaller Au-NP size. In particular, SiO_2@g-C_3N_4 with 0.5 % Au sample has remarkably homogeneous size distribution. The increase of volume to surface ratio confers very small Au NPs with added reactivity [44,45] as they have been found to have electrochemical and optical properties that are both shape and size dependent [46].

Traditional routes for Au NPs preparation such as impregnation, coprecipitation or ion exchange usually lead to larger particle sizes (>20 nm) with dissimilar exposed facets on the semiconductors, both factors not favorable for neither the LSPR effect nor the charge carrier transfer [31].

The introduction of gold NPs in the structures may confer an improvement on their optical absorption properties. The UV–vis diffuse reflectance spectra of SiO_2@g-C_3N_4 and g-C_3N_4 with Au 0.5/1% are shown in Fig. 5a and b, respectively. In all cases the mayor absorption band is located below 450 nm, there is no significant changes on this limit with the addition of the NPs, as the gold was not incorporated in the lattice of the g-C_3N_4 sample, but deposited on its surface [47]. A peak located at over 500 nm (500–530 range) was observed in the samples

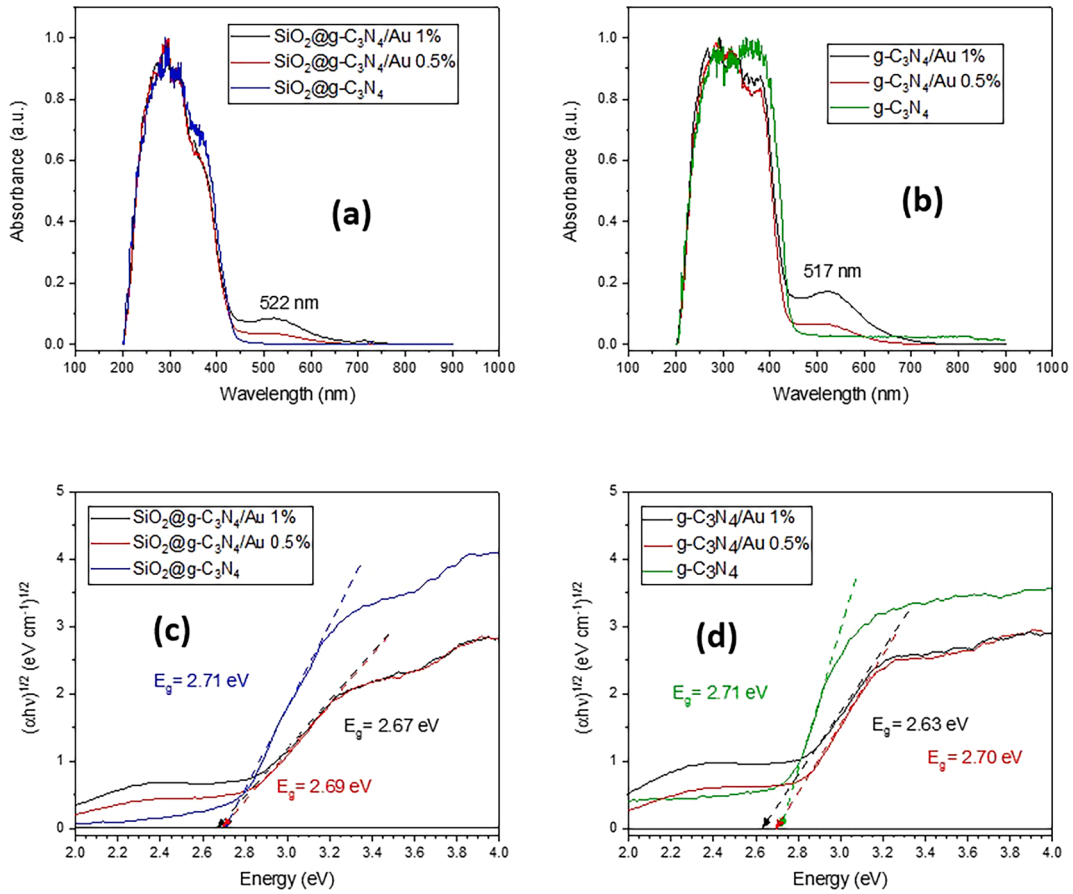

Fig. 5. Diffuse reflectance UV–vis spectrum of the samples with their Tauc plot as an inset.

with gold, originating from the surface plasmon resonance of the NPs [39,48] as it was not present in the starting samples. As expected, this peak is stronger the higher the concentration in gold [40]. The carbon nitride series displays more absorbance especially the sample with 1 % gold which could be related to the fact that metallic gold appears in PXRD diffractogram in this series. The light harvesting activity of the NPs is expected to enhance the photocatalytic activity performance [49]. The band gaps of the samples, based on Tauc plots, are shown in Fig. 5c and d. Both SiO_2@g-C_3N_4 and g-C_3N_4 present the same band gap, of 2.71 eV. Although this value could enable them to harvest sunlight, it still differs from the ideal band gap of a semiconductor of around 2.0 eV [50]. Thus, obtaining a narrower bandgap is one of the main goals to be achieved through the material modification. The heterojunction between the semiconductor and the gold NPs produces a slight decrease in the band gap of all the samples. SiO_2@g-C_3N_4 with 0.5 % and 1 % Au have a 2.69 and 2.67 eV band gap, respectively, while in the case of g-C_3N_4 samples with 0.5 % and 1 % Au their band gap is of 2.70 and 2.63 eV. The surface plasmon resonance effect of the NPs is responsible for the reduced E_g, which can make the material more responsible to solar light [51].

The surface composition and chemical state of the as-synthesized samples was further examined with XPS analysis. Fig. 6a displays the survey spectra of the four samples. The g-C_3N_4 samples show almost no oxygen and peaks corresponding to C, N and Au. The latter peak is more prominent in the sample with 1 % Au. The samples with nanotubes as a support show also peaks corresponding to both silicon and oxygen, these two elements represent more than 30 % of the surface composition of both samples. The total percentage of each element present in the surface of the four samples is collected in Table 2. Gold nanoparticles represent the 0.7–0.8 % in the samples with 0.5 % of gold and 1.6 % in the samples with 1 % gold, disclosing that nanoparticles stay in the surface of the catalysts in a greater proportion and are thus available to help in the photoreaction. The high resolution spectra of the two Au 4f peaks, are represented in Fig. 6b and are all situated at 84 and 87.7 eV, corresponding to Au4f 7/2 and 5/2 respectively and mark the presence of only metallic gold in the samples [43,52]. The methodology utilized for the decoration of the samples with gold nanoparticles is thereby solid and reliable, as the results obtained are consistent. Fig. 6c displays the high-resolution XPS spectrum for the C1s region, fitted into three peaks. The most intense peak, located at between 287.6 and 287.8 eV corresponds to the sp^2 carbon atoms in the g-C_3N_4 triazine units (C-N=C). The peak associated with the C–C bonds is located at 284.5 eV. The high-resolution spectra of the N 1 s region (Fig. 6d) shows three major peaks situated at around 398.3, 399.3 and 400.5 eV which correspond to sp^2 N atoms in the triazine unit (C-N=C), N atoms between aromatic rings (tertiary N-$(C)_3$ groups) and the presence of $–NH_2$ groups, respectively [53,54]. The presence of gold has not led to a substantial increase on the binding energies of both C and N 1 s spectra, when comparing to pristine g-C_3N_4 and SiO_2-C_3N_4 [51], although in the samples with nanotubes, a small increase on the biding energies of the samples has been recorded when the gold percentage has increased from 0.5 to 1. Fig. 6e showcases the high-resolution spectra of O 1 s which only represents a 2.4–2.7 % in the samples with no nanotubes. In samples with SiO_2, this percentage rises up to 26 %, and the binding energy of O 1 s is slightly displaced to higher energies, 532.7–532.8 eV, representative of SiO_2 binding. Si 2p spectra is represented in Fig. 6f, silicon represents around 9 % of the samples with nanotubes and its binding energy is situated in the 103.4–103.5 eV range which corresponds to a silica chemical bond.

Photoluminescence (PL) studies were used to investigate the recombination process of the electron-hole pairs photogenerated in the semiconductor. Fig. 7 shows the PL spectra of the samples performed at

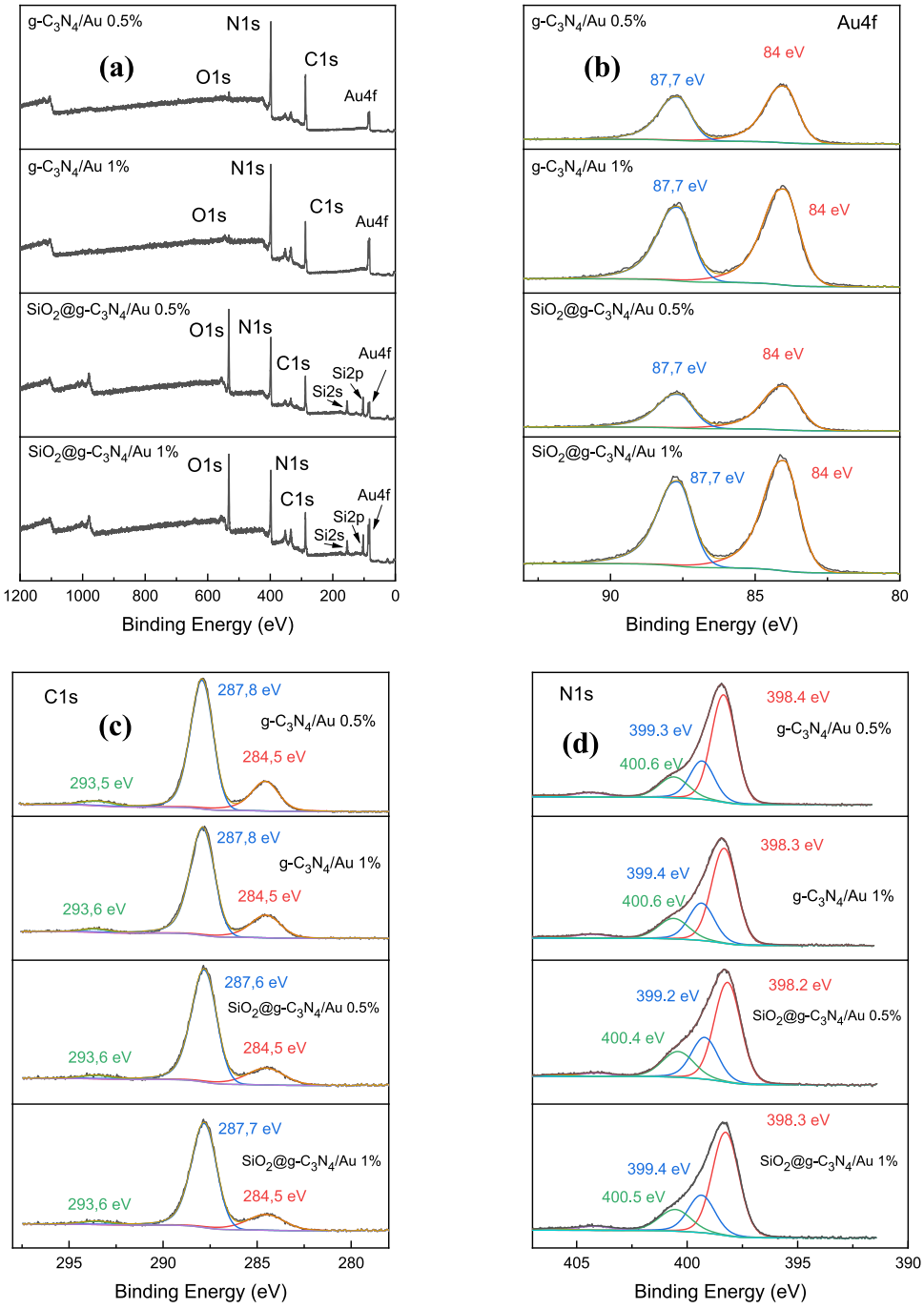

Fig. 6. XPS survey, Au 4f, C 1 s, N 1 s, O 1 s and Si 2p spectra of the g-C_3N_4/Au and SiO_2@g-C_3N_4/Au samples.

room temperature and under an excitation wavelength of 365 nm: Fig. 7a for SiO_2@g-C_3N_4 and **7b** for g-C_3N_4 samples. A higher intensity would indicate a quicker recombination efficiency of the charge carriers. The presence of gold NPs on the surface of the samples contributed to the restraining of the photo-generated e^-- h^+ recombination. The intensity decreased in the order: g-C_3N_4/Au 0.5 % > g-C_3N_4/Au 1 % > SiO_2@g-C_3N_4/Au 1 % > SiO_2@g-C_3N_4/Au 0.5 %. Nanotube-containing samples had a starting vantage point, as the presence of the nanotubes reduced significantly the carriers' recombination. Au NPs inhibit the recombination of the charge carriers and promote a better separation of the electron-hole pairs while also being responsible for a better light harvesting, leading to an enhancement of the catalytic photoactivity of the samples. Results obtained in the PL spectral pattern perfectly match the catalytic activity of the samples. In the g-C_3N_4 series, the quenching of the signal is slightly greater in the sample containing 1 % Au while in the SiO_2@g-C_3N_4 series, the 0.5 % Au-sample performs better. The presence of gold in the samples seems to slightly displace the emission peak to lower wavelengths. The percentage of gold chosen for the samples seems to have been appropriately selected. Samples with higher amounts of gold nanoparticles are usually found to start to produce a lower decrease in the intensity of the emission peak [39,40].

3.2. *Amoxicillin photodegradation performance*

Studies in the absence of light were performed simultaneously to those with the UV or visible light in order to address the possible

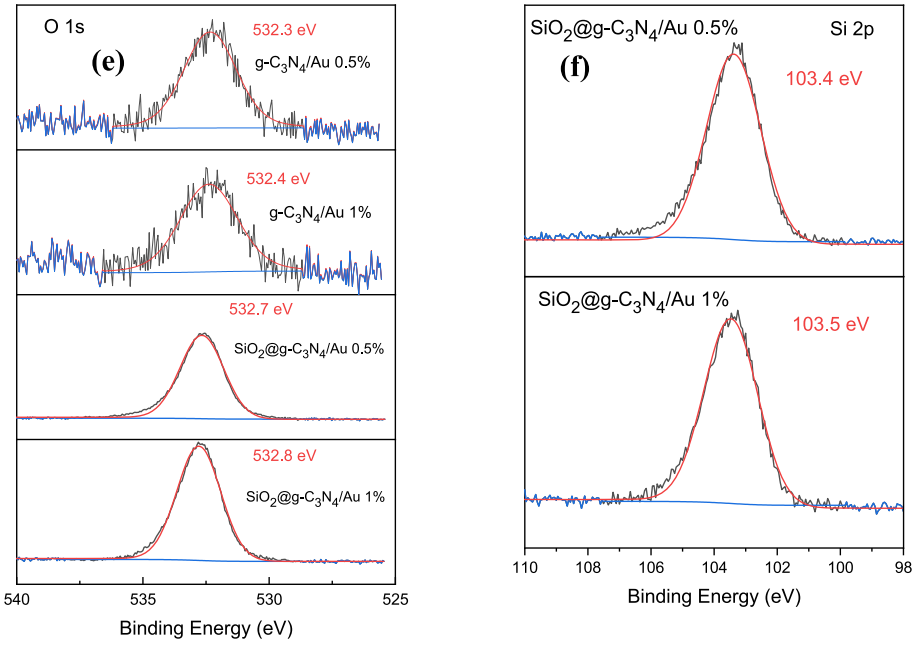

Fig. 6. (*continued*).

Table 2
Surface composition of the (SiO_2 nanotubes)@g-C_3N_4 samples with either 0.5 or 1 % of gold nanoparticles.

Element	g-C_3N_4 + Au 0.5 %	g-C_3N_4 + Au 1 %	SiO_2@g-C_3N_4 + Au 0.5 %	SiO_2@g-C_3N_4 + Au 1 %
C	45.6	44.2	29	29.6
O	2.7	2.4	26	22.7
N	50.9	51.8	34.6	37.5
Si	––	–—	9.7	8.6
Au	0.8	1.6	0.7	1.6

catalyst-contaminant adsorption mechanism. All samples failed to adsorb any amoxicillin. Considering the pk_a of amoxicillin [55], when the pH is close to 7, used in our experiments, amoxicillin is almost fully negatively charged whereas silica nanotubes are also negatively charged, thus preventing the adsorption from appearing. Fig. 8 shows the results obtained when using SiO_2@g-C_3N_4 sample without light and with either UV or visible light. UV light was effective in removing amoxicillin from the sample in less than two hours and although visible light worked at first, it seems to stall pass the 60 min mark.

The decoration of the composites with gold nanoparticles was next tried in order to improve the catalysts efficacy when under visible light. Au percentages chosen were 0.5 and 1 % as these outperform lower or higher percentages [39,40,56]. Results obtained of both the SiO_2@g-C_3N_4 and the g-C_3N_4 series with 0 %, 0.5 % and 1 % are displayed in Fig. 9. Gold NPs samples ameliorate the results obtained with samples before the noble metal decoration, however the sample SiO_2@g-C_3N_4/Au 1 % fails to obtain the results of SiO_2@g-C_3N_4 in the first 60 min. In the series with no nanotubes, both Au samples outperform the g-C_3N_4 starting sample, and the g-C_3N_4/Au 0.5 % degrades more than 40 % of amoxicillin in the first two hours (against the 27 % obtained by g-C_3N_4/Au 1 %). Overall, sample SiO_2@g-C_3N_4/Au 0.5 % provides the best performance, 52 % degradation of amoxicillin vs. 21 % obtained with the other nanotubes' samples. The pseudo-first-order kinetics of the samples are represented in Fig. 10. Sample SiO_2@g-C_3N_4/Au 0.5 % has the highest rate constant, at 0.0068 min^{-1}, the other two nanotubed samples (with no gold and 1 % NPs) have similar rate constants with 0.0027 and 0.0025 min^{-1}, respectively. Sample with only g-C_3N_4 obtains the lowest value, at 0.0019 min^{-1} and sample g-C_3N_4/Au 0.5 %

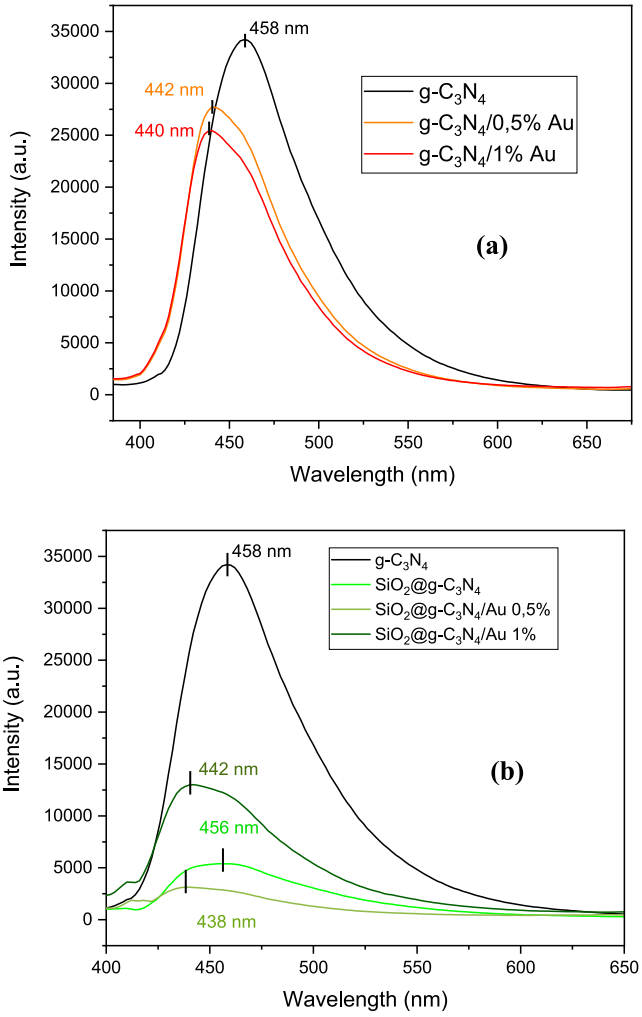

Fig. 7. Photoluminescent spectra of g-C_3N_4 and the SiO_2@g-C_3N_4 nanohybrid with different percentages of Au NPs.

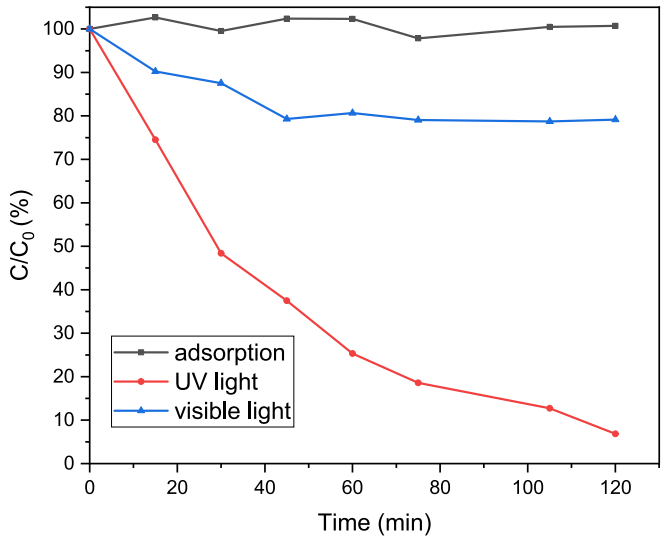

Fig. 8. Amoxicillin adsorption and visible or UV lamp degradation behavior of SiO_2@g-C_3N_4 (without gold NPs) sample.

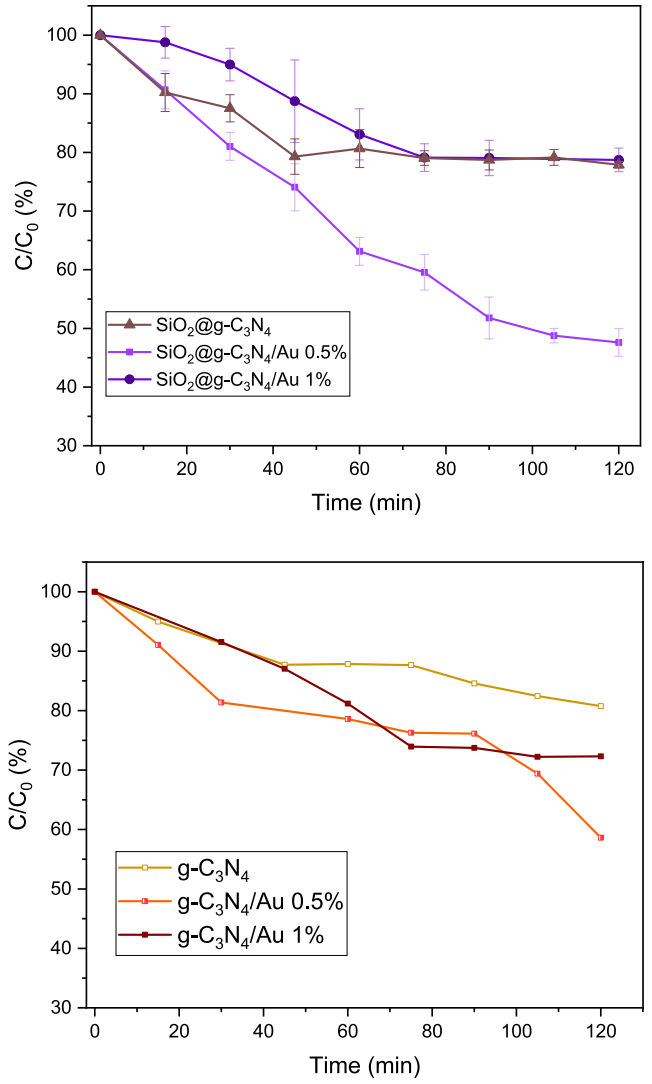

Fig. 9. Degradation behavior of SiO_2@g-C_3N_4 and g-C_3N_4 samples.

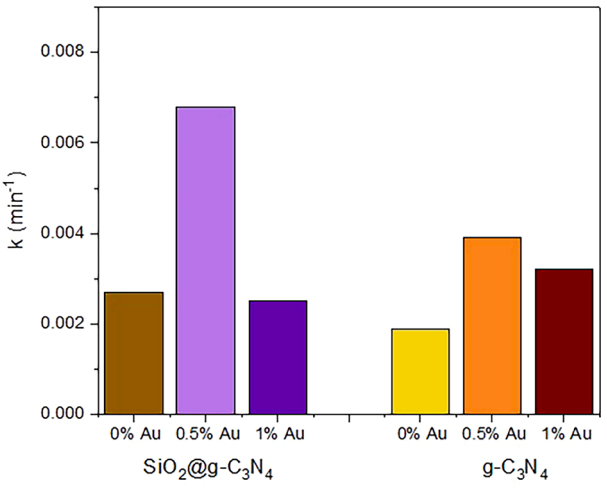

Fig. 10. pseudo-first-order kinetics of the samples for amoxicillin degradation.

succeeds in doubling its reaction kinetics results with a 0.0039 min^{-1} rate. Overall, the better performance obtained with SiO_2@g-C_3N_4/Au 0.5 % seems to be a product of both a bigger BET surface, which could signify a greater probability of pollutant-catalyst interaction, and the lowest electron-hole pair recombination, as seen in the PL emission results. These two factors are a direct consequence of the introduction of the SiO_2 nanotubes and gold nanoparticles in the system. The percentage of gold that gives the best results seems to vary with the synthesis method and, even though usually situated in the 0.5–1 % region, is difficult to predict in advance the best result within this range.

The antibiotic amoxicillin bears several organic functional groups such as carboxylate (—COOH), amino (—NH_2), hydroxyl (—OH) or thioether (−S-). In the case of Au NPs, previous reports show that all these functional groups can interact with the nanoparticle surface. In the case of the g-C_3N_4 surface or the available SiO_2 surface, the amoxicillin molecules would interact through hydrogen bonding between its functional groups such as carboxylate (—COOH), amino (—NH_2), hydroxyl (—OH) and the —NH_2 or OH groups at the surface. Therefore, in the Scheme 1 we show a general interaction between the amoxicillin and the surface, where the photocatalytic process takes place.

For the study of amoxicillin degradation, carbon nitride has been combined with a second semiconductor (TiO_2, ZnO, MoS_2, Fe_2O_3) another carbon-based material such as graphene oxide or with noble metals, such as silver. A comparison of the kinetic results obtained with the different modifications of C_3N_4 while trying to improve its photocatalytical performance is shown in Table 3. Kinetic values obtained highlight the recalcitrance of this antibiotic to being degraded. To our knowledge, the effect of gold nanoparticles on carbon nitride has not been tested for amoxicillin degradation although it has been proven successful with dyes such as methylene blue [40] and rhodamine B [48] or drugs such as paracetamol [43] or antibiotic tetraclycine hydrochloride [57].

Study of the degradation process.

Trapping experiments were performed to specify the most relevant active species in the degradation process. Tert-butanol, triethanolamine and an inert N_2 atmosphere were introduced in the reaction to capture hydroxyl radicals ($OH^{\bullet}$), photogenerated holes (h^+) and superoxide radicals ($\bullet O_2^-$), respectively. The formation of the active species is limited to the band gap of the semiconductor employed, their potentials have to be included in the semiconductor E_{VB}-E_{CB} limits (around 1.60 eV- -1.11 eV for the SiO_2@g-C_3N_4/Au 0.5 % sample, 2.69 band gap see Scheme 2). When using carbon nitride as semiconductor, the direct formation of hydroxyl radicals (2.4 eV) is not allowed, as its potential is not included in the E_{VB}-E_{CB} interval. Results obtained are represented in Fig. 11: the presence of triethanolamine, trapping photogenerated holes,

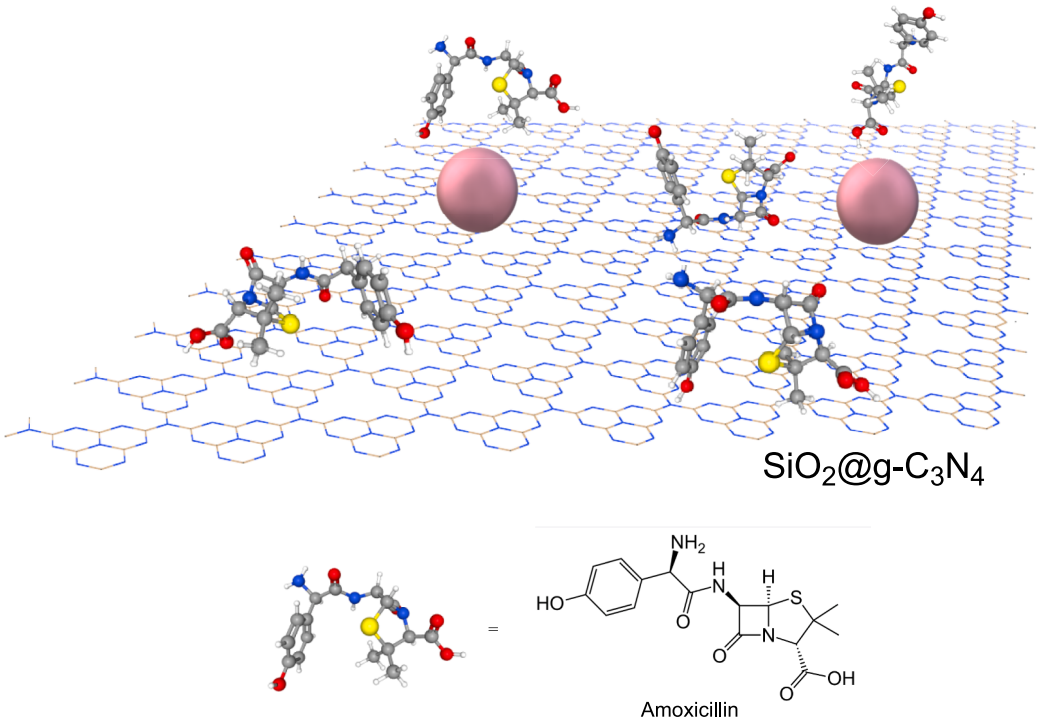

Scheme 1. Interaction mechamism of the SiO_2@g-C_3N_4 /Au sample with amoxicillin.

Table 3
Pseudo-first-order kinetics of g-C_3N_4 composites in Amoxicillin degradation.

Sample	Pseudo-first-order kinetic (min^{-1})	Conditions	Reference
Fe_3O_4 NPs/g-C_3N_4	0.0215	0.25 mM AMOX 1 g/L catalysts UV light 500 W halogen lamp	[64]
TiO_2	0.00078	20 ppm AMOX, 4 g/L	[65]
g-C_3N_4	0.00127	catalyst	
g-C_3N_4/ TiO_2	0.00134	vis light	
Ag-TiO_2	0.00180	500 W	
Ag/g-C_3N_4/ TiO_2	0.00340	tungsten–halogen lamp	
Ag/TiO_2/M−g−C_3N_4	0.0614	5 ppm AMOX,	[63]
B-g- C_3N_4	0.00495	1 g/L catalyst, vis light 300 W xenon lamp	
g-C_3N_4/MoS_2 (3 %)	0.0575	15 ppm AMOX, 0.5 g/L catalyst,	[66]
g-C_3N_4	0.0075	vis light 300 W Xe lamp	
Ag/g-C3N4/ZnO	0.00166	40 ppm amox, 0.08 g/L catalyst vis light 300 W lamp	[62]
RGO@g-C_3N_4/$BiVO_4$	0.0556	10 ppm AMOX, 1 g/L catalyst vis light 500 W halogen lamp	[67]
g-C_3N_4	0.0019	5 ppm AMOX,	This work
g-C_3N_4/SiO_2 nanotubes_Au0.5 %	0.0068	1 g/L catalyst, vis light 124 W LED lamp	

clearly affects the degrading process and the nitrogen atmosphere, quenching the formation of $\bullet O_2^-$, has a similar outcome. Thus, the amoxicillin degradation process is a combination of the photogenerated holes and the superoxide radicals. This results clearly display the effect

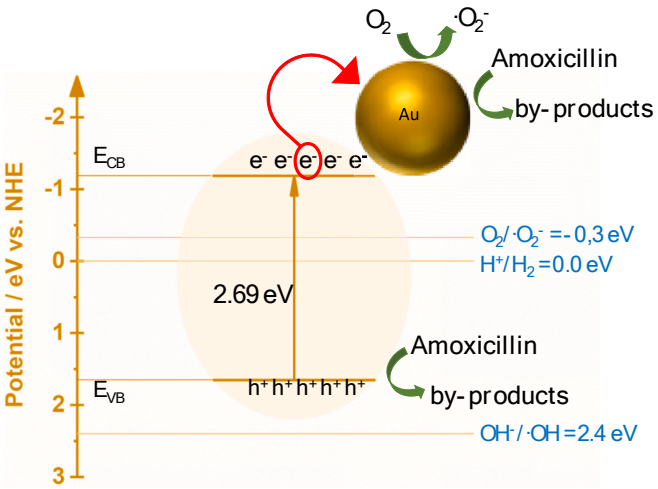

Scheme 2. Degradation active species in the SiO_2@g-C_3N_4 /Au 0.5 % sample.

caused by the gold nanoparticles in the catalyst performance: when the SiO_2@g-C_3N_4 composite (with no nanoparticles) was studied for the degradation of norfloxacin antibiotic [24] only the use of triethanolamine for trapping the holes (h^+) had a significant effect on the catalyst performance, the addition of Au NPs, displays a combination of both h^+ and $\bullet O_2^-$, making the nanoparticles responsible for the superoxide generation. The presence of the gold on the surface of the semiconductor nanosheets modified the degradation mechanism, as they are polarized in charge and absorbed and scattered the incident visible light as a result of their strong LSPR [58]. Plasmonic photocatalysts come from the Au Fermi level presence between the CB and the VB of the carbon nitride [39,59]. Under sunlight irradiation, electrons released from the CB of the semiconductor can be captured by the NPs, an easily reduce nearby O_2 into $\bullet O_2^-$. The presence of the Au NPs-C_3N_4 system has previously been reported to combine both h^+ and $\bullet O_2^-$ as active species responsible

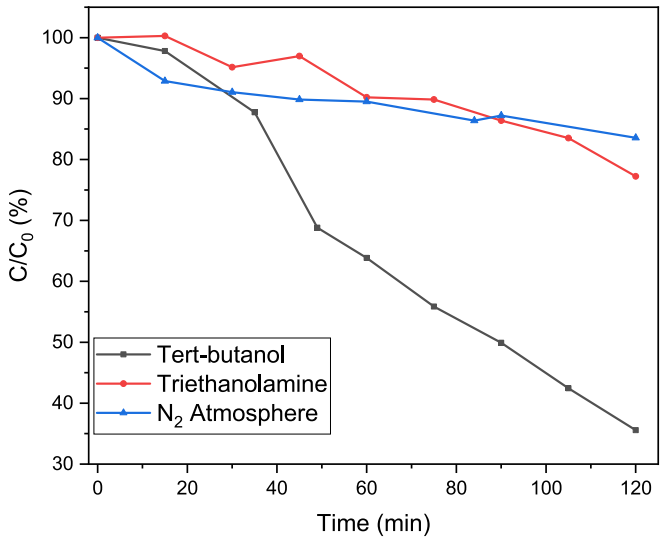

Fig. 11. Trapping experiments performed on SiO_2@g-C_3N_4/Au 0.5 % sample. Tert-butanol: scavengers for hydroxyl radicals ($OH^{\bullet}$). Triethanolamine: scavenger for photogenerated holes (h^+). Inert N_2 atmosphere to quench superoxide radicals ($\cdot O_2^-$).

for the degradation of Rhodamine B and methylene blue [39,40]. The present work demonstrates and further confirms that the presence of Au NPs in the catalyst generates the superoxide radicals ($\bullet O_2^-$). This group has reported results that go in line with these for the degradation of ciprofloxacin: the use of g-C_3N_4 on its own showcases that holes are the only active species responsible [60] or a combination of Au-Ag NPs with N-doped carbon/TiO_2 uses a combination of holes and $\bullet O_2^-$. However, some authors obtained different results: *Nguyen et al.* [61] report only the presence of only superoxide radicals when using silver NPs in a C_3N_4/halloysite composite for the degradation of tetracycline and other studies report the presence of subsidiary hydroxyl radicals ($OH^{\bullet}$) generated either from the presence of ZnO in the C_3N_4 composite [62] or from the $\bullet O_2^-$ [51,63], the last one also stating that the TiO_2/C_3N_4 combination is responsible for the generation of superoxide radicals.

4. Summary and conclusions

This work reports the effect of gold nanoparticles in a silica nanotubes/C_3N_4 composite for the degradation of the antibiotic amoxicillin under visible light. Two different percentages of gold were tested (0.5 and 1 wt%) using [Au(C_6F_5)(tht)] as organometallic precursor which is reduced in the presence of the SiO_2@g-C_3N_4 nanotube system. This controlled synthesis process resulted in small (<10 nm) gold nanoparticles, homogenously deposited throughout the samples. Results obtained showcase the importance of the gold amount in the sample as 0.5 % Au delivered the best results: the SiO_2@g-C_3N_4/Au 0.5 % NPs had a pseudo-first-grade kinetic constant 3.5 times larger than g-C_3N_4 and 2.5 times that of SiO_2@g-C_3N_4. Trapping experiments showed that both holes (h^+) and superoxide radicals ($\bullet O_2^-$) performed in the SiO_2-C_3N_4/Au 0.5 % NPs degradation of amoxicillin with the gold nanoparticles being responsible for both the production of superoxide radicals and the reduction of electron-hole recombination.

CRediT authorship contribution statement

L. Santamaría: Writing – original draft, Investigation, Formal analysis, Data curation. **S.A. Korili:** Writing – review & editing, Supervision. **A. Gil:** Writing – review & editing, Supervision, Funding acquisition. **J.M. López-de-Luzuriaga:** Writing – review & editing, Supervision, Resources, Funding acquisition. **M. Monge:** Writing – review & editing, Supervision, Methodology, Conceptualization.

Declaration of competing interest

The authors declare that they have no known competing financial interests or personal relationships that could have appeared to influence the work reported in this paper.

Data availability

No data was used for the research described in the article.

Acknowledgements

J. M. L. L. and M.M. thank the DGI MICINN/FEDER (project number PID2022-139739NB-I00 (AEI/FEDER, UE)) and by "ERDF A way of making Europe". Authors from Universidad Pública de Navarra are grateful for financial support from the Spanish Ministry of Science and Innovation (AEI/MINECO) through project PID2020-112656RBC21. L. S. thanks the Universidad Pública de Navarra for a post-doctoral Margarita Salas grant, financed by the European Union-Next Generation EU. The authors also acknowledge the use of instrumentation as well as the technical advice provided by the National Facility ELECMI ICTS, node "Laboratorio de Microscopias Avanzadas" at Universidad de Zaragoza.

References

[1] European Commission, Commission Directive 2014/101/EU of 30 October 2014 amending Directive 2000/60/EC of the European Parliament and of the Council establishing a framework for Community action in the field of water policy, Off. J. Eur. Union. L311 (2014) 32–35.
[2] European Commission, Commission implementing decision (EU) 2018/840 of 5 June 2018 establishing a watch list of substances for Union-wide monitoring in the field of water policy pursuant to Directive 2008/105/EC of the European Parliament and of the Council and repealing Comm, Off. J. Eur. Union. L 141 (2018) 9–12.
[3] European Commission, Communication from the commission to the Council and the European Parliament. A European One Health Action Plan againsnt Antimicrobial Resistance, https://Ec.Europa.Eu/Health/Antimicrobial-Resistance/Eu-Action-on-Antimicrobial-Resistance_Es. (2017) 1–20.
[4] WHO, Antimicrobial Resistance Global Report on Surveillance, 2014. https://doi.org/10.1002/9781119680642.ch16.
[5] J. O'Neill. (2016) Tackling drug-resistant infections globally: final report and recommendations. DOI: APO-63983.
[6] A. García-Reiriz, P.C. Damiani, A.C. Olivieri, Different strategies for the direct determination of amoxicillin in human urine by second-order multivariate analysis of kinetic-spectrophotometric data, Talanta 71 (2007) 806–815, https://doi.org/10.1016/j.talanta.2006.05.050.
[7] L.O. Omuferen, B. Maseko, J.O. Olowoyo, Occurrence of antibiotics in wastewater from hospital and convectional wastewater treatment plants and their impact on the effluent receiving rivers: current knowledge between 2010 and 2019, Environ. Monit. Assess. 194 (2022), https://doi.org/10.1007/s10661-022-09846-4.
[8] E.O. Ezugbe, S. Rathilal, Membrane technologies in wastewater treatment: a review, Membranes (Basel). 10 (2020), https://doi.org/10.3390/membranes10050089.
[9] X. Liu, R. Ma, L. Zhuang, B. Hu, J. Chen, X. Liu, X. Wang, Recent developments of doped g-C3N4 photocatalysts for the degradation of organic pollutants, Crit. Rev. Environ. Sci. Technol. 51 (2021) 751–790, https://doi.org/10.1080/10643389.2020.1734433.
[10] Y. Wang, S. Shen, Progress and prospects of non-metal doped graphitic carbon nitride for improved photocatalytic performances, Wuli Huaxue Xuebao/ Acta Phys - Chim. Sin. 36 (2020) 1–14, https://doi.org/10.3866/PKU.WHXB201905080.
[11] D.T.C. Minh, T. Do Dat, T.T. Quan, N.T.H. Nam, Q. Thi Thanh Huong, N.M. Dat, N. H. Hieu, Phyto-synthesis of tin oxide nanoparticles using Diospyros mollis leaves extract doped graphitic carbon nitride for photocatalytic methylene blue degradation and hydrogen peroxide production, Colloids Surfaces A Physicochem. Eng. Asp. 687 (2024) 133454, https://doi.org/10.1016/j.colsurfa.2024.133454.
[12] T.T. Buu, N.D. Hai, C.Q. Cong, N.T.H. Nam, T.D. Khoa, D.G. Vy, N.T. Nguyen, D.T. Y. Oanh, N.H. Hieu, A case study of different bismuth oxyhalides BiOX (X = F, Cl, Br, and I)/biochar-derived rice husk@graphitic carbon nitride for the robustness of H2O2 photoproduction and antibiotic photodegradation, J. Water Process Eng. 57 (2024), https://doi.org/10.1016/j.jwpe.2023.104558.
[13] T.T. Buu, C.Q. Cong, V.M. Quan, B.K. Ngoc, N.T.H. Nam, L.T.P. Thao, D.H.M. Tam, L.G. Han, N.H. Hieu, Construction of Z-scheme heterojunction TiO2-ZnO@Oxygen-doped gC3N4 composite for enhancing H2O2 photoproduction and removal of pharmaceutical pollutants under visible light, Surf. Interfaces 43 (2023) 103516, https://doi.org/10.1016/j.surfin.2023.103516.

[14] R. Ratshiedana, A.T. Kuvarega, A.K. Mishra, Titanium dioxide and graphitic carbon nitride–based nanocomposites and nanofibres for the degradation of organic pollutants in water: a review, Environ. Sci. Pollut. Res. 28 (2021) 10357–10374, https://doi.org/10.1007/s11356-020-11987-3.
[15] A. Sudhaik, P. Raizada, P. Shandilya, D.Y. Jeong, J.H. Lim, P. Singh, Review on fabrication of graphitic carbon nitride based efficient nanocomposites for photodegradation of aqueous phase organic pollutants, J. Ind. Eng. Chem. 67 (2018) 28–51, https://doi.org/10.1016/j.jiec.2018.07.007.
[16] Z. Sun, C. Li, X. Du, S. Zheng, G. Wang, Facile synthesis of two clay minerals supported graphitic carbon nitride composites as highly efficient visible-light-driven photocatalysts, J. Colloid Interface Sci. 511 (2018) 268–276, https://doi.org/10.1016/j.jcis.2017.10.005.
[17] C. Li, N. Zhu, S. Yang, X. He, S. Zheng, Z. Sun, D.D. Dionysiou, A review of clay based photocatalysts: role of phyllosilicate mineral in interfacial assembly, microstructure control and performance regulation, Chemosphere 273 (2021) 129723, https://doi.org/10.1016/j.chemosphere.2021.129723.
[18] H. Abdullah, D.H. Kuo, Photocatalytic performance of the SiO2 sphere/n-type TiO2/p-type CuBiS2 composite catalysts coated with different contents of Ag nanoparticles under ultraviolet and visible light irradiations, Appl. Phys. A Mater. Sci. Process. 122 (2016) 1–11, https://doi.org/10.1007/s00339-016-0261-y.
[19] B. Mazinani, A. Beitollahi, A.K. Masrom, L. Samiee, Z. Ahmadi, Synthesis and photocatalytic performance of hollow sphere particles of SiO2-TiO2 composite of mesocellular foam walls, Ceram. Int. 43 (2017) 11786–11791, https://doi.org/10.1016/j.ceramint.2017.06.017.
[20] Y. Xu, W. Zheng, W. Liu, Enhanced photocatalytic activity of supported TiO2: dispersing effect of SiO2, J. Photochem. Photobiol. A Chem. 122 (1999) 57–60, https://doi.org/10.1016/S1010-6030(98)00470-5.
[21] H.J. Kim, Y.G. Shul, H. Han, Photocatalytic properties of silica-supported TiO2, Top. Catal. 35 (2005) 287–293, https://doi.org/10.1007/s11244-005-3836-y.
[22] L. Peng, Z.W. Li, R.R. Zheng, H. Yu, X.T. Dong, Preparation and characterization of mesoporous g-C3N4/SiO2 material with enhanced photocatalytic activity, J. Mater. Res. 34 (2019) 1785–1794, https://doi.org/10.1557/jmr.2019.113.
[23] X. Wang, S. Wang, W. Hu, J. Cai, L. Zhang, L. Dong, L. Zhao, Y. He, Synthesis and photocatalytic activity of SiO2/g-C 3N4 composite photocatalyst, Mater. Lett. 115 (2014) 53–56, https://doi.org/10.1016/j.matlet.2013.10.016.
[24] M.M. Santamaría, L. Korili S.A, A. Gil, J.M. López-de-Luzuriaga, Synthesis of high-surface-area C3N4 deposited on halloysite-derived silica nanotubes: enhanced visible light degradation of norfloxacin, Catal. Today. (2024), https://doi.org/10.1016/j.cattod.2024.114584.
[25] E. Alwin, R. Wojcieszak, K. Kočí, M. Edelmannová, M. Zieliński, A. Suchora, T. Pędziński, M. Pietrowski, Reductive modification of carbon nitride structure by metals—the influence on structure and photocatalytic hydrogen evolution, Materials (Basel). 15 (2022), https://doi.org/10.3390/ma15030710.
[26] S. Zhang, P. Gu, R. Ma, C. Luo, T. Wen, G. Zhao, W. Cheng, X. Wang, Recent developments in fabrication and structure regulation of visible-light-driven g-C3N4-based photocatalysts towards water purification: a critical review, Catal. Today. 335 (2019) 65–77, https://doi.org/10.1016/j.cattod.2018.09.013.
[27] D. Zhu, Q. Zhou, Nitrogen doped g-C3N4 with the extremely narrow band gap for excellent photocatalytic activities under visible light, Appl. Catal. B Environ. 281 (2021) 119474, https://doi.org/10.1016/j.apcatb.2020.119474.
[28] L. Jiang, X. Yuan, Y. Pan, J. Liang, G. Zeng, Z. Wu, H. Wang, Doping of graphitic carbon nitride for photocatalysis: a reveiw, Appl. Catal. B Environ. 217 (2017) 388–406, https://doi.org/10.1016/j.apcatb.2017.06.003.
[29] Y. Chang, Z. Liu, X. Shen, B. Zhu, D.K. Macharia, Z. Chen, L. Zhang, Synthesis of Au nanoparticle-decorated carbon nitride nanorods with plasmon-enhanced photoabsorption and photocatalytic activity for removing various pollutants from water, J. Hazard. Mater. 344 (2018) 1188–1197, https://doi.org/10.1016/j.jhazmat.2017.10.040.
[30] Z. Guo, F. Dai, H. Yin, M. Zhang, J. Xing, L. Wang, The dual role of Au nanoparticles in the surface plasmon resonance enhanced photocatalyst Au/g-C3N4, Colloids Interface Sci. Commun. 48 (2022) 100615, https://doi.org/10.1016/j.colcom.2022.100615.
[31] L. Li, Q. Zhang, X. Wang, J. Zhang, H. Gu, W.L. Dai, Au nanoparticles embedded in carbon self-doping g-C3N4: facile photodeposition method for superior photocatalytic H2Evolution, J. Phys. Chem. C. 125 (2021) 10964–10973, https://doi.org/10.1021/acs.jpcc.1c02269.
[32] W. Ge, K. Liu, S. Deng, P. Yang, L. Shen, Z-scheme g-C3N4/ZnO heterojunction decorated by Au nanoparticles for enhanced photocatalytic hydrogen production, Appl. Surf. Sci. 607 (2023) 155036, https://doi.org/10.1016/j.apsusc.2022.155036.
[33] Y. Zhang, F. Mao, H. Yan, K. Liu, H. Cao, J. Wu, D. Xiao, A polymer–metal–polymer–metal heterostructure for enhanced photocatalytic hydrogen production, J. Mater. Chem. A. 3 (2015) 109–115, https://doi.org/10.1039/C4TA04636F.
[34] R. Usón, A. Laguna, J. Vicente, Preparation and properties of stable salts containing mono- or bis-(pentafluorophenyl)aurate(I) and mono-, tris-, or tetrakis-(pentafluorophenyl)aurate(III) ions, J. Chem. Soc. Chem. Commun. (1976) 353–354, https://doi.org/10.1039/C39760000353.
[35] Z. Yang, J. Yan, J. Lian, H. Xu, X. She, H. Li, g-C3N4/TiO2 nanocomposites for degradation of ciprofloxacin under visible light irradiation, ChemistrySelect 1 (2016) 5679–5685, https://doi.org/10.1002/slct.201600861.
[36] H. Wang, J. Li, C. Ma, Q. Guan, Z. Lu, P. Huo, Y. Yan, Melamine modified P25 with heating method and enhanced the photocatalytic activity on degradation of ciprofloxacin, Appl. Surf. Sci. 329 (2015) 17–22, https://doi.org/10.1016/j.apsusc.2014.12.049.
[37] N. Lu, P. Wang, Y. Su, H. Yu, N. Liu, X. Quan, Construction of Z-Scheme g-C3N4/RGO/WO3 with in situ photoreduced graphene oxide as electron mediator for efficient photocatalytic degradation of ciprofloxacin, Chemosphere 215 (2019) 444–453, https://doi.org/10.1016/j.chemosphere.2018.10.065.
[38] M. Thommes, K. Kaneko, A.V. Neimark, J.P. Olivier, F. Rodriguez-Reinoso, J. Rouquerol, K.S.W. Sing, Physisorption of gases, with special reference to the evaluation of surface area and pore size distribution (IUPAC Technical Report), Pure Appl. Chem. 87 (2015) 1051–1069, https://doi.org/10.1515/pac-2014-1117.
[39] S. Tonda, S. Kumar, V. Shanker, Surface plasmon resonance-induced photocatalysis by Au nanoparticles decorated mesoporous g-C3N4 nanosheets under direct sunlight irradiation, Mater. Res. Bull. 75 (2016) 51–58, https://doi.org/10.1016/j.materresbull.2015.11.011.
[40] M. Faisal, M. Jalalah, F.A. Harraz, A.M. El-Toni, A. Khan, M.S. Al-Assiri, Au nanoparticles-doped g-C3N4 nanocomposites for enhanced photocatalytic performance under visible light illumination, Ceram. Int. 46 (2020) 22090–22101, https://doi.org/10.1016/j.ceramint.2020.05.250.
[41] M. Faisal, M.A. Rashed, J. Ahmed, M. Alsaiari, M. Jalalah, S.A. Alsareii, F. A. Harraz, Au nanoparticles decorated polypyrrole-carbon black/g-C3N4 nanocomposite as ultrafast and efficient visible light photocatalyst, Chemosphere 287 (2022) 131984, https://doi.org/10.1016/j.chemosphere.2021.131984.
[42] L. Deng, P. Yuan, D. Liu, P. Du, J. Zhou, Y. Wei, Y. Song, Y. Liu, Effects of calcination and acid treatment on improving benzene adsorption performance of halloysite, Appl. Clay Sci. 181 (2019) 105240, https://doi.org/10.1016/j.clay.2019.105240.
[43] M. Jiménez-Salcedo, M. Monge, M.T. Tena, An organometallic approach for the preparation of Au–TiO2 and Au-g-C3N4 nanohybrids: improving the depletion of paracetamol under visible light, Photochem. Photobiol. Sci. 21 (2022) 337–347, https://doi.org/10.1007/s43630-022-00172-9.
[44] B. Yoon, H. Häkkinen, U. Landman, A.S. Wörz, J.M. Antonietti, S. Abbet, K. Judai, U. Heiz, Charging effects on bonding and catalyzed oxidation of CO on Au8 clusters on MgO, Science 307 (2005) 403–407, https://doi.org/10.1126/science.1104168.
[45] T. Bhowmik, M.K. Kundu, S. Barman, Ultra small gold nanoparticles-graphitic carbon nitride composite: an efficient catalyst for ultrafast reduction of 4-nitrophenol and removal of organic dyes from water, RSC Adv. 5 (2015) 38760–38773, https://doi.org/10.1039/c5ra04913j.
[46] R.C. Pawar, S. Kang, S.H. Ahn, C.S. Lee, Gold nanoparticle modified graphitic carbon nitride/multi-walled carbon nanotube (g-C3N4/CNTs/Au) hybrid photocatalysts for effective water splitting and degradation, RSC Adv. 5 (2015) 24281–24292, https://doi.org/10.1039/c4ra15560b.
[47] Y. Wang, R. Shi, J. Lin, Y. Zhu, Enhancement of photocurrent and photocatalytic activity of ZnO hybridized with graphite-like C3N4, Energy Environ. Sci. 4 (2011) 2922–2929, https://doi.org/10.1039/C0EE00825G.
[48] X. Zhou, G. Zhang, C. Shao, X. Li, X. Jiang, Y. Liu, Fabrication of g-C3N4/SiO2-Au composite nanofibers with enhanced visible photocatalytic activity, Ceram. Int. 43 (2017) 15699–15707, https://doi.org/10.1016/j.ceramint.2017.08.130.
[49] X. Zhou, Y. Wang, Y. Wang, M. Zhang, H. Gao, X. Zhang, Superior uniform carbon nanofibers@g-C3N4 core-shell nanostructures embedded by Au nanoparticles for high-efficiency photocatalyst, J. Hazard. Mater. 388 (2020) 121759, https://doi.org/10.1016/j.jhazmat.2019.121759.
[50] H. Li, Z. Zhang, Y. Liu, W. Cen, X. Luo, Functional group effects on the HOMO–LUMO gap of g-C3N4, Nanomaterials 8 (2018) 4–9, https://doi.org/10.3390/nano8080589.
[51] X. Huang, N. Zhu, F. Mao, Y. Ding, S. Zhang, F. Li, H. Liu, P. Wu, Novel Au@C modified g-C3N4 (Au@C/g-C3N4) as efficient visible-light photocatalyst for toxic organic pollutant degradation: synthesis, performance and mechanism insight, Sep. Purif. Technol. 252 (2020), https://doi.org/10.1016/j.seppur.2020.117485.
[52] C. Zhu, L. Han, P. Hu, S. Dong, In situ loading of well-dispersed gold nanoparticles on two-dimensional graphene oxide/SiO2 composite nanosheets and their catalytic properties, Nanoscale 4 (2012) 1641–1646, https://doi.org/10.1039/c2nr11625a.
[53] A. Thomas, A. Fischer, F. Goettmann, M. Antonietti, J.O. Müller, R. Schlögl, J. M. Carlsson, Graphitic carbon nitride materials: Variation of structure and morphology and their use as metal-free catalysts, J. Mater. Chem. 18 (2008) 4893–4908, https://doi.org/10.1039/b800274f.
[54] X. Wang, Q. Liu, Q. Yang, Z. Zhang, X. Fang, Three-dimension g-C3N4 aggregate composed of hollow bubbles with high activity for photocatalytic degradation of tetracycline, Carbon N. Y. 136 (2018) 103–112, https://doi.org/10.1016/j.carbon.2018.04.059.
[55] C. Homsirikamol, N. Sunsandee, U. Pancharoen, K. Nootong, Synergistic extraction of amoxicillin from aqueous solution by using binary mixtures of Aliquat 336, D2EHPA and TBP, Sep. Purif. Technol. 162 (2016) 30–36, https://doi.org/10.1016/j.seppur.2016.02.003.
[56] H. Wang, T. Sun, L. Chang, P. Nie, X. Zhang, C. Zhao, X. Xue, The g-C 3 N 4 nanosheets decorated by plasmonic Au nanoparticles: a heterogeneous electrocatalyst for oxygen evolution reaction enhanced by sunlight illumination, Electrochim. Acta. 303 (2019) 110–117, https://doi.org/10.1016/j.electacta.2019.02.061.
[57] J. Xue, S. Ma, Y. Zhou, Z. Zhang, M. He, Facile photochemical synthesis of Au/Pt/g-C3N4 with plasmon-enhanced photocatalytic activity for antibiotic degradation, ACS Appl. Mater. Interfaces. 7 (2015) 9630–9637, https://doi.org/10.1021/acsami.5b01212.
[58] S. Samanta, S. Martha, K. Parida, Facile synthesis of Au/g-C3N4 nanocomposites: an inorganic/organic hybrid plasmonic photocatalyst with enhanced hydrogen gas evolution under visible-light irradiation, ChemCatChem 6 (2014) 1453–1462, https://doi.org/10.1002/cctc.201300949.
[59] Y. Ide, F. Liu, J. Zhang, N. Kawamoto, K. Komaguchi, Y. Bando, D. Golberg, Hybridization of Au nanoparticle-loaded TiO2 with BN nanosheets for efficient

solar-driven photocatalysis, J. Mater. Chem. A. 2 (2014) 4150–4156, https://doi.org/10.1039/C3TA13769D.
[60] M. Jiménez-Salcedo, M. Monge, M.T. Tena, Study of intermediate by-products and mechanism of the photocatalytic degradation of ciprofloxacin in water using graphitized carbon nitride nanosheets, Chemosphere 247 (2020), https://doi.org/10.1016/j.chemosphere.2020.125910.
[61] H.T. Nguyen, H.V. Doan, T.T.B. Nguyen, X.N. Pham, Nanoarchitectonics of Ag-modified g-C3N4@halloysite nanotubes by a green method for enhanced photocatalytic efficiency, Adv. Powder Technol. 33 (2022) 103862, https://doi.org/10.1016/j.apt.2022.103862.
[62] N.Q. Thang, A. Sabbah, L.C. Chen, K.H. Chen, C.M. Thi, P. Van Viet, High-efficient photocatalytic degradation of commercial drugs for pharmaceutical wastewater treatment prospects: a case study of Ag/g-C3N4/ZnO nanocomposite materials, Chemosphere 282 (2021) 130971, https://doi.org/10.1016/j.chemosphere.2021.130971.
[63] B. Gao, J. Wang, M. Dou, C. Xu, X. Huang, Enhanced photocatalytic removal of amoxicillin with Ag/TiO2/mesoporous g-C3N4 under visible light: property and mechanistic studies, Environ. Sci. Pollut. Res. 27 (2020) 7025–7039, https://doi.org/10.1007/s11356-019-07112-8.
[64] A. Mirzaei, Z. Chen, F. Haghighat, L. Yerushalmi, Magnetic fluorinated mesoporous g-C3N4 for photocatalytic degradation of amoxicillin: transformation mechanism and toxicity assessment, Appl. Catal. B Environ. 242 (2019) 337–348, https://doi.org/10.1016/j.apcatb.2018.10.009.
[65] K.H. Leong, S.L. Liu, L.C. Sim, P. Saravanan, M. Jang, S. Ibrahim, Surface reconstruction of titania with g-C 3 N 4 and Ag for promoting efficient electrons migration and enhanced visible light photocatalysis, Appl. Surf. Sci. 358 (2015) 370–376, https://doi.org/10.1016/j.apsusc.2015.06.184.
[66] M. Govinda raj, E. Vijayakumar, R. Preetha, M.G. Narendran, G. Abigail Jennifer, E. Varathan, B. Neppolian, V.K. Ganesh, A. John Bosco, Experimental investigation into the π-conjugated HT-g-C3N4/MoS2 (X) evokes the electron transport in type-II heterojunction to achieve high photocatalytic antibiotic removal under visible-light irradiation, Sep. Purif. Technol. 292 (2022) 121028, https://doi.org/10.1016/j.seppur.2022.121028.
[67] M.F.R. Samsudin, S. Sufian, Hybrid 2D/3D g-C3N4/BiVO4 photocatalyst decorated with RGO for boosted photoelectrocatalytic hydrogen production from natural lake water and photocatalytic degradation of antibiotics, J. Mol. Liq. 314 (2020), https://doi.org/10.1016/j.molliq.2020.113530.